NOAA Technical Memorandum ERL ARL-31

U.S. DEPARTMENT OF COMMERCE
NATIONAL OCEANIC AND ATMOSPHERIC ADMINISTRATION
Environmental Research Laboratories

Computed Response of Tetrahedral Constant-Density Balloons to Vertical Sinusoidal and Helical Air Motions

WALTER H. HOECKER
STEVEN R. HANNA

Air Resources
Laboratories
SILVER SPRING,
MARYLAND
April 1971

RONMENTAL RESEARCH LABORATORIES

AIR RESOURCES LABORATORIES

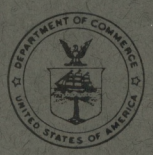

IMPORTANT NOTICE

Technical Memoranda are used to insure prompt dissemination of special studies which, though of interest to the scientific community, may not be ready for formal publication. Since these papers may later be published in a modified form to include more recent information or research results, abstracting, citing, or reproducing this paper in the open literature is not encouraged. Contact the author for additional information on the subject matter discussed in this Memorandum.

NATIONAL OCEANIC AND ATMOSPHERIC ADMINISTRATION

U.S. DEPARTMENT OF COMMERCE
National Oceanic and Atmospheric Administration
Environmental Research Laboratories

NOAA Technical Memorandum ERL ARL-31

COMPUTED RESPONSE OF TETRAHEDRAL CONSTANT-DENSITY BALLOONS TO VERTICAL SINUSOIDAL AND HELICAL AIR MOTIONS

Walter H. Hoecker

Air Resources Trajectory Laboratory, Silver Spring, Maryland

Steven R. Hanna

Atmospheric Turbulence and Diffusion Laboratory, Oak Ridge, Tennessee

This work performed, in part, on the basis of research sponsored by the AEC (Division of Biology and Medicine and Reactor Development and Technology) and EPA (Air Pollution Control Office).

Air Resources Laboratories
Silver Spring, Marlyand
April 1971

TABLE OF CONTENTS

ABSTRACT

The quantitative response of some particular examples of constant density balloons to vertical sinusoidal and helical atmospheric oscillations has been estimated by using a digital computer to solve the equation of motion for the balloon. Results were obtained for wave periods of 4 to 48 minutes, velocity amplitudes of 0.3 to 3.5 meters per second, and wave amplitudes of 10 to 1600 meters. For vertical air motions, phase lead angle decreases and amplitude response increases as atmospheric stability, balloon radius, and air period decrease, and as vertical air speed and drag coefficient increase. For a typical wave of 15 minutes period and 300 meters amplitude, the phase lead is only 5% of the wave length and amplitude response is 94%. A rearrangement of the equation allows an estimation of the trajectory of the air parcel, initially associated with the balloon, from the radar-tracked balloon movements.

For helical air motions that are characterized entirely as solid rotation, or are irrotational with a solid rotation core, the balloon eventually spirals into the center of the helix provided the helix is sufficiently long and persists for sufficient time. For helical motions in which the air speed is dependent only on time, the balloon track becomes elliptical.

It is clear from these studies that care must be exercised in interpreting constant level balloon data. Statistics involving the vertical fluctuations of the balloon may not be related to similar statistics for the air. However, it is suggested that the air motions can be estimated from the balloon motions through the solution of the equation of motion.

COMPUTED RESPONSE OF TETRAHEDRAL CONSTANT-DENSITY BALLOONS TO VERTICAL SINUSOIDAL AND HELICAL AIR MOTIONS

Walter H. Hoecker and S. R. Hanna

1. INTRODUCTION

Constant-density balloons are being used increasingly as Lagrangian air parcel tracers (Angell & Pack, 1960; Angell, Pack, and Dickson, 1968; Vergeiner and Lilly, 1970). They are particularly suited for areas where use of stationary wind-measuring equipment is impractical. Low-stretch Mylar plastic is used in their construction and very often they are shaped as tetrahedrons (tetroons) because of relatively low manufacturing costs and ease of shipping and handling. Radar and visual observations show that these "tetroons" are quite responsive to vertical air currents. Consequently they have also been used to estimate Reynolds stress, production of eddy kinetic energy, etc., from time-dependent balloon movements. The accuracy of these derived statistics depends on how effectively the balloon responds to atmospheric motions encountered in flight.

In another paper (Hanna & Hoecker, 1971), balloon response to vertical sinusoidal air waves was computed by analytical and digital solutions to the equation of motion. Balloon phase-lead angle and the ratio of the magnitudes of balloon velocity to air wave velocity were shown to be dependent on the speed amplitude and period of the air motions, the atmospheric stability, the radius of the balloon, and the drag coefficient.

The present paper gives some examples of balloon response for the typical balloons used by the Air Resources Laboratories of The National Oceanic and Atmospheric Administration. Methods of estimating air parcel trajectories and vertical air velocities from observed balloon motions are

given. In addition, the response of the balloon to vertical-lateral helical air currents is computed for several amplitude-period combinations and types of helical motions.

2. THE EQUATION OF MOTION

The differential equation of motion for the balloon is:

$$M_b\ddot{Z}_b = \frac{1}{2}\rho_a C_d A(\dot{Z}_a - \dot{Z}_b)|\dot{Z}_a - \dot{Z}_b| + g(\rho_a V_b) - M_b g$$
$$+(\rho_a V_b)\ddot{Z}_a - M_{ap}(\ddot{Z}_b - \ddot{Z}_a) \qquad (1)$$

with terms representing, from left to right, the following forces: total force on the balloon, drag, static buoyancy, gravity, dynamic buoyancy, and acceleration drag forces. The symbols key is shown in Table 1. It is assumed that the scales of air motion are much greater than the size of the balloon. Equation (1) differs from those used by others(Hirsch and Booker, 1966; MacCready 1964; Mangold, 1966; Reed, 1963; Scoggins, 1967) by the inclusion of the dynamic buoyancy term, $(\rho_a V_b)\ddot{Z}_a$. Its magnitude at cycle peaks is equal to the static buoyancy for air periods T of about 4.5 minutes but decreases with longer periods. It is about 1/9th the static buoyancy for T = 15 min., for example.

Prandtl (1952) decribes the principle of the dynamic buoyancy force, and the acceleration drag force that opposes it. In order to isolate the effects of these two forces, he assumes that the drag, static buoyancy, and gravity forces are zero. His expression for the combined effect is:

$$\rho_a V_b \ddot{Z}_a - \rho_a(\ddot{Z}_b - \ddot{Z}_a)V_b' = \rho_b V_b \ddot{Z}_b$$

Table 1. List of Symbols

M_b	= Mass of system (gm)(balloon, enclosed gases, transponder, fastenings, etc.)
M_{ap}	= Added mass, or apparent mass (gm).
ρ_a	= Air density (gm cm^{-3}).
Z_b	= Vertical position of balloon (cm).
$\dot{Z}_b$	= Vertical speed of balloon (cm sec^{-1}).
$\ddot{Z}_b$	= Vertical acceleration of balloon (cm sec^{-2}).
$\dot{Z}_a$	= Vertical wind speed (cm sec^{-1}).
$\ddot{Z}_a$	= Vertical wind acceleration (cm sec^{-2}).
C_d	= Coefficient of form drag.
A	= Cross-section area of balloon (cm^2).
V_b	= Volume of balloon (cm^3).
g	= Acceleration of gravity (980 cm sec^{-1}).
W_a	= Velocity amplitude of air wave (cm sec^{-1}).
T	= Period of air-motion wave (sec).
A_a	= Air-motion amplitude (cm).
W_b	= Velocity amplitude of balloon (cm sec^{-1}).
A_b	= Balloon trajectory amplitude (cm).
s	= Stability parameter (t^{-2}).
R	= Balloon radium (cm).
ϕ	= Phase lead angle (deg).
$(\dot{Z}_a - \dot{Z}_b)$	= Relative air speed past balloon (cm sec^{-1}).

which becomes,

$$\ddot{Z}_b = \ddot{Z}_a \frac{V_b + V_b'}{V_b(\rho_b/\rho_a) + V_b'} \qquad (2)$$

and which gives the acceleration of the balloon in terms of the ambient atmospheric acceleration. Here V_b' is the volume of the "apparent mass" which influences the acceleration drag. The following conclusions may be drawn from (2):

for $\rho_a < \rho_b$, $\ddot{Z}_a > \ddot{Z}_b$

for $\rho_a = \rho_b$, $\ddot{Z}_a = \ddot{Z}_b$

for $\rho_a > \rho_b$, $\ddot{Z}_a < \ddot{Z}_b$

Thus the balloon accelerates faster than the air, and in the same direction, when the balloon density is less than the ambient air density. This effect can be demonstrated by the following simple laboratory experiment: A piece of wax or paraffin, which is a little less dense than water, is placed in a 4' x 1-1/2" glass tube. The tube is completely filled with water, and securely corked with all bubbles excluded. The piece of wax is allowed to float to one end of the tube by tilting it. Then the tube is held horizontally and rotated perpendicular to its long axis in a horizontal plane. As rotation continues, the piece of wax migrates toward the axis of rotation and eventually comes to rest near the axis. Although the piece of wax pushes outward on the fluid with its force of reaction, the centripetal force of the fluid on the piece of wax is greater causing the wax to move to the center of the tube. This demonstration of the principles in (2) can easily be performed in the classroom.

By algebraic rearrangement equation (1) becomes:

$$\ddot{Z}_b = \frac{(M_{ap} + \rho_a V_b)\ddot{Z}_a}{(M_b + M_{ap})} + \frac{\rho_a C_d A(\dot{Z}_a - \dot{Z}_b)\left|\dot{Z}_a - \dot{Z}_b\right|}{2(M_b + M_{ap})} + \frac{g(\rho_a V_b - M_b)}{(M_b + M_{ap})} \qquad (3)$$

which is the working equation used here. Air density and displaced mass $\rho_a V_b$ are allowed to vary linearly with the height of the tetroon. For simplicity the apparent mass M_{ap} was assumed to be a fixed fraction of M_s, whereas it is actually a fraction of $(\rho_a V_b)$. It can be shown that this arrangement causes a negligible difference in the results. The lapse rate of helium was allowed for by the application of the gas laws in the inflation and balloon-lift equations and tables developed by Delver and Booth (1965).

3. RESULTS FOR VERTICAL AIR MOTIONS

A CDC 6600 computer at Suitland, Maryland, was used to compute the response of the balloon to atmospheric sine waves (both horizontal and vertical) with velocity amplitudes W_a of 30 to 350 cm sec^{-1} and periods of oscillation T of 4 to 48 minutes. For most combinations of velocity amplitude (W_a) and period (T), a form-drag coefficient of 0.80 and the 1962 U. S. Standard Atmosphere were used. Expansion and contraction of the balloon for decreasing and increasing external pressure and ambient temperature changes were allowed for by using Delver and Booth's (1965) measurements; in the computations it was assumed that there was no pressure-volume hysteresis in the balloon. A constant stepwise computational time-interval of 2 sec. was used except for the longest period and largest velocity amplitudes where a one-second interval was used.

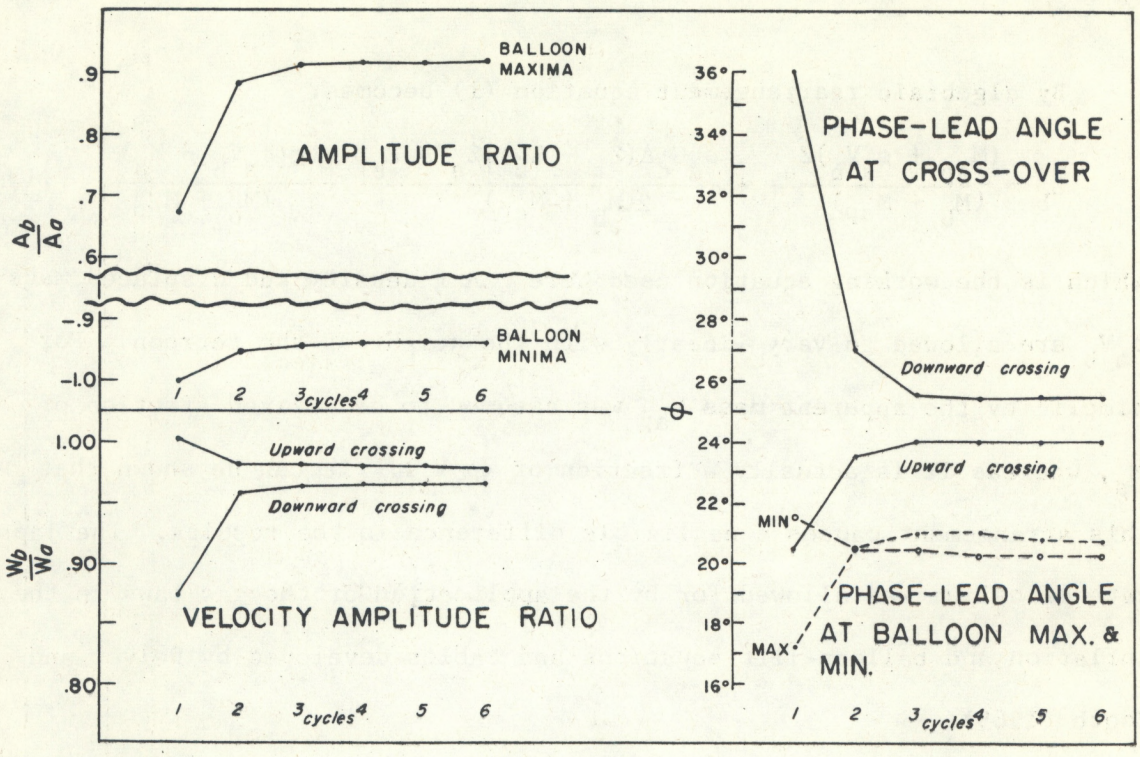

Figure 1: The computed adjustment of the balloon to a typical daytime, sinusoidal atmospheric wave in the vertical plane. The wave period is 24 minutes, amplitude is 460 meters, velocity amplitude is 2.0 m s^{-1}, and balloon drag coefficient is 0.8. Additional details are found in the text.

Each computation was started with balloon and air parcel positions and speeds equal. It was necessary to carry the computation through only three cycles because of the rapid convergence of the balloon into an equilibrium oscillation. Figure 1 illustrates the adjustment of the balloon into an equilibrium condition for a typical daytime atmospheric oscillation (T = 24 min, W_a = 200 cm sec^{-1}) completed through 6 cycles. For the items (amplitude, phase lead, etc.,) used in the figure, most of the adjustment of the balloon is accomplished by the second cycle and virtually no change occurs after the third cycle.

In all of the computations it is assumed that the balloon is imbedded in a layer of air moving in wave-like motions as if flowing over a series of mountain ranges and having no vertical variation in horizontal or vertical motion.

3.1 Examples of Computed Vertical Balloon Trajectories

Some representative computed responses of the balloon to vertical sinusoidal air motions are shown in figure 2, where a drag coefficient of 0.80 was used. Height and time values have been normalized for easy comparison. The balloon track showing the poorest amplitude response and largestphase lead is associated with the air wave with the longest period (48 min.) and smallest velocity amplitude (30 cm sec^{-1}). The inflection in the curve near phase angle 110° for the trajectory associated with T = 48 min and W_a = 30 cm sec^{-1}, is a result of the balloon's crossing the equilibrium level at about the time that vertical air motion has ceased. Momentum, provided by downward buoyancy force, carries the balloon downward across the equilibrium level. Then, upward-directed drag plus upward-directed buoyancy forces slow the balloon's descent until about 130° phase angle. At about this point the downward velocity of the air increases sufficiently to overcome any upward relative velocity caused by the upward-directed buoyancy force. Such reactions occur after each crossing of the equilibrium level by the balloon and an inflection is noted there. Because of the initial conditions that were used, the balloon typically climbs in the first and second cycles as shown by the increasing elevation of succeeding wave maxima and minima. Most of the climbing occurs between the first and second cycle.

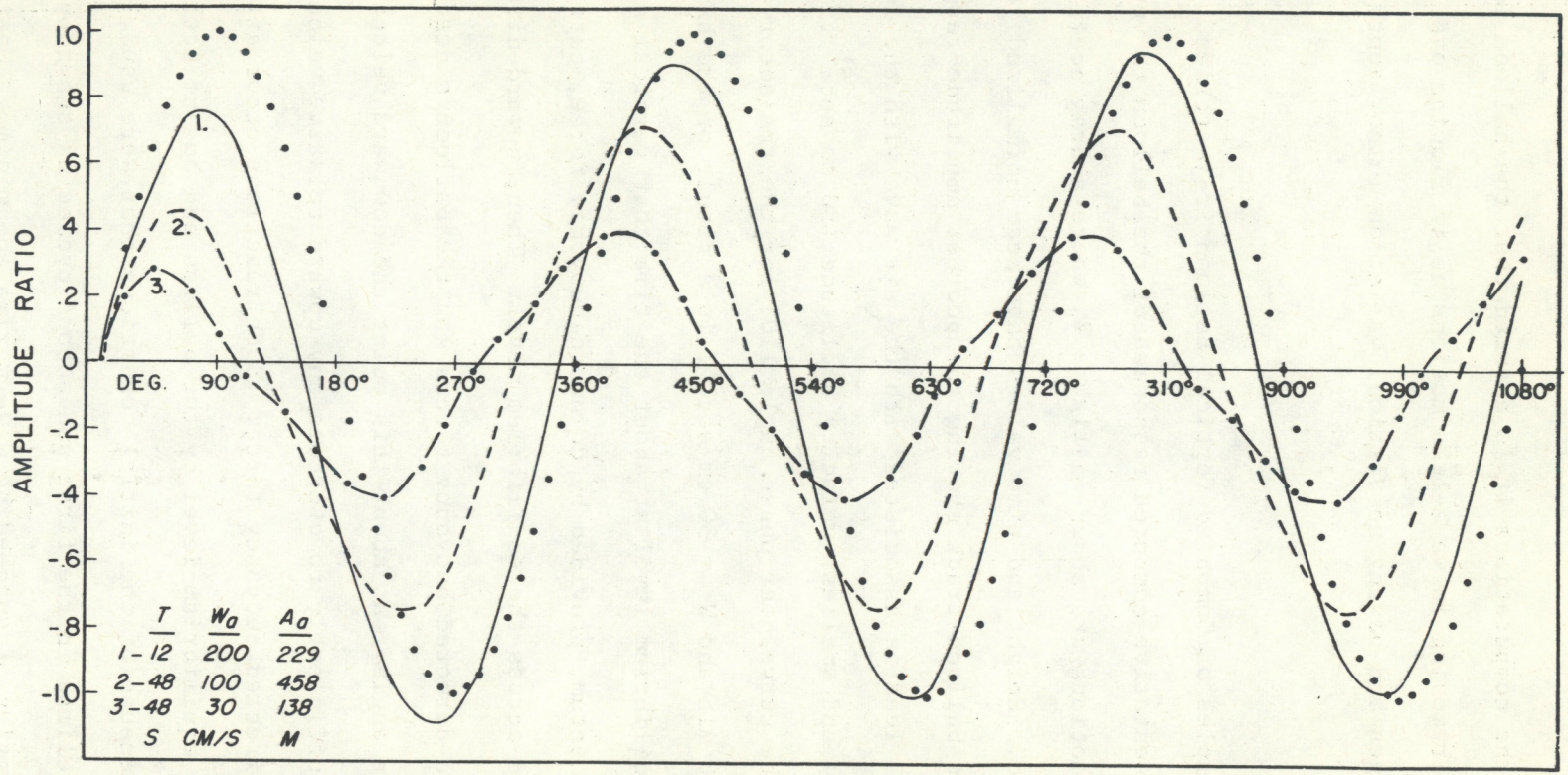

Figure 2: Computed balloon response in the vertical plan to three combinations of period and velocity amplitude selected to show results of combining long-period oscillations with small velocity amplitudes and vice versa. The inflections on curve "3" near the equilibrium level are explained in the text. Dots represent parcel wave.

3.2 General Performance

The general problem of balloon response to vertical sinusoidal air motions was analyzed by Hanna and Hoecker (1971). It was found that the phase lead angle ϕ and magnitude response W_b/W_a were functions only of a single dimensionless number for air periods T greater than the natural Brunt-Vaisala period $2\pi s^{-1/2}$, where s is a stability parameter defined by:

$$s = \frac{g}{\rho_b} \frac{\partial}{\partial z} (\rho_b - \rho_a)$$

When the air period T approaches the Brunt-Vaisala period of the balloon, the magnitude response W_b/W_a exceeds unity. The dimensionless number that acts as the sole independent variable in this problem is the product:

$$\frac{sRT}{C_d W_a}$$

The functional relationships $\phi(sRT/C_dW_a)$ and $W_b/W_a(sR(T-10s^{-1/2})/C_dW_a)$ are plotted in figures 3 and 4. The empirical factor $10s^{-1/2}$ is close to the Brunt-Vaisala period. The following general conclusions can be drawn from these graphs:

Response increases when
- stability s decreases
- radius R decreases
- period T decreases
- drag coef. C_d increases
- speed W_a increases

Some examples of the response characteristics of specific balloons are given in the next few paragraphs.

3.3 Specific Results

Twenty-eight computations were made combining four air velocity-amplitude classes with seven period-classes in order to cover a wide range of atmospheric conditions. In all cases typical balloons used by the Air Resources Laboratories were used to determine the parameters of the problem. The range of air motion corresponds to the range observed by these balloons. Air velocity-amplitudes (W_a) used were 30, 100, 200, and 350 cm sec^{-1}, and wave periods T used were 4, 6, 12, 15, 24, 36, and 48 minutes. Efficiencies (ϕ, W_b/W_a and A_b/A_a) were estimated in the third cycle of the computation where the balloon had reached an equilibrium with the air-motion wave. Since the balloon phase lead angle ϕ varies slightly throughout the cycle, this angle was taken as the average of lead at wave maximum and minimum and at the downward and upward crossings of the equilibrium level by the balloon. The balloon amplitude used in the amplitude ratio A_b/A_a was the average of the absolute values of the maximum balloon excursions from the equilibrium level. The efficiency data are presented in figures 5, 6, and 7. When plotted in dimensionless form, these data agree with the curves in figures 3 and 4.

Phase-lead angle ϕ as a function of period T for the four speed-amplitude classes discussed earlier are shown in figure 5. In each speed-amplitude class, longer periods increase the phase-lead angle which lowers the balloon's tracking efficiency Note that $\Delta\phi/\Delta T$ is greater for lower velocity-amplitude classes. If the four curves were extrapolated toward shorter periods, they would intersect at about T = 1.5 minutes at which point phase-lead efficiency would be independent

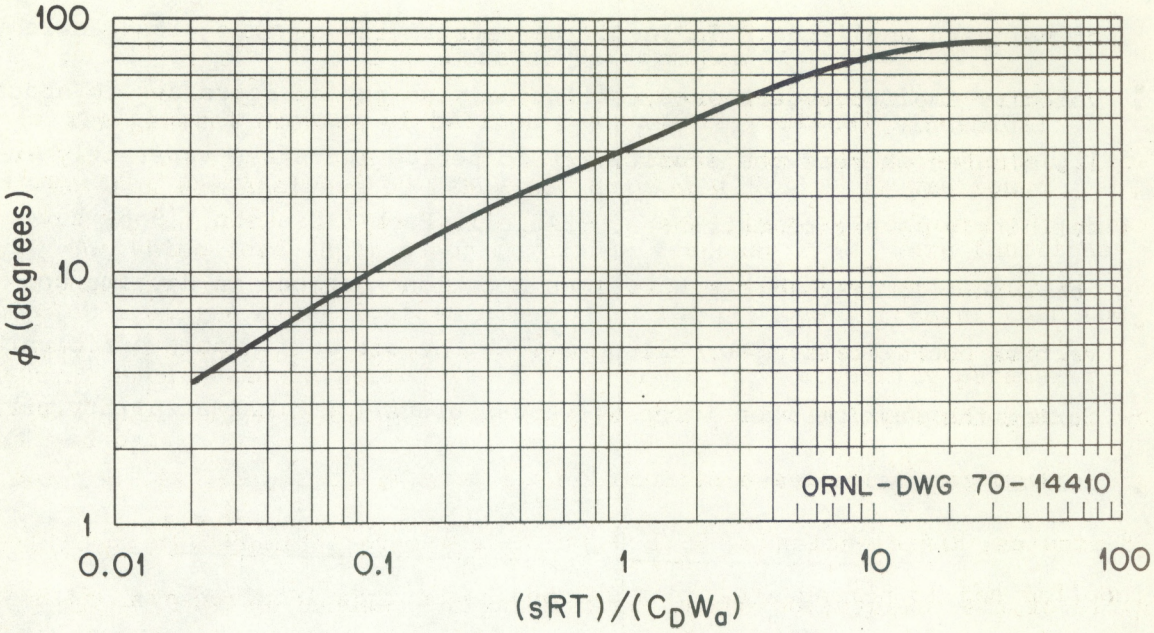

Figure 3: The phase lead angle ø as a function of the dimensionless number $sRT/C_d W_a$. The symbols are explained in table 1.

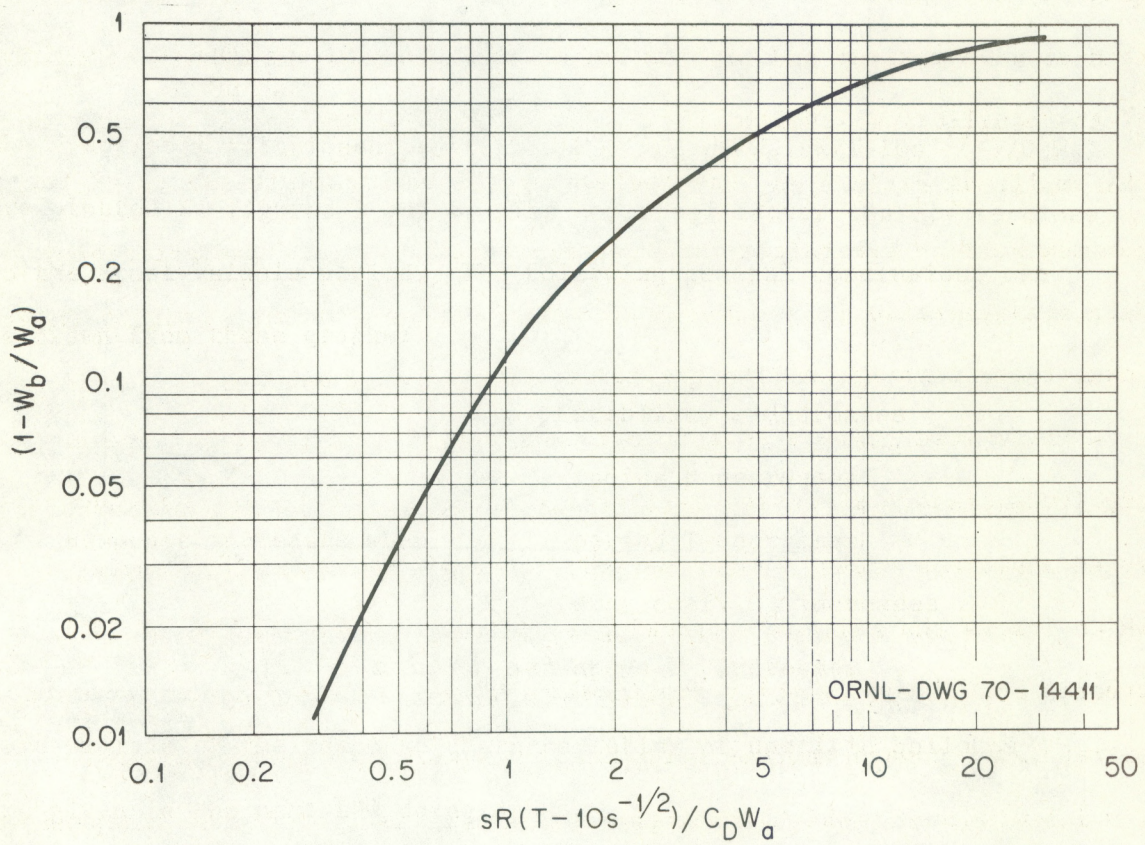

Figure 4: The decrease in speed magnitude $(1-W_b/W_a)$ as a function of the dimensionless number $sR(T-10s^{-\frac{1}{2}})/C_d W_a$. The symbols are explained in table 1.

of velocity amplitude. In fact, the sensitivity of phase-lead angle to velocity amplitude decreases continuously as period decreases to about 1.5 minutes whereas the sensitivity to period increases apparently indefinitely as period decreases. Angell, Pack & Dickson (1968) have observed relatively large W_a values with long periods in daytime convective conditions. The balloon tracks the air motion more efficiently during the daytime when large W_a values prevail and the stability parameter s is small.

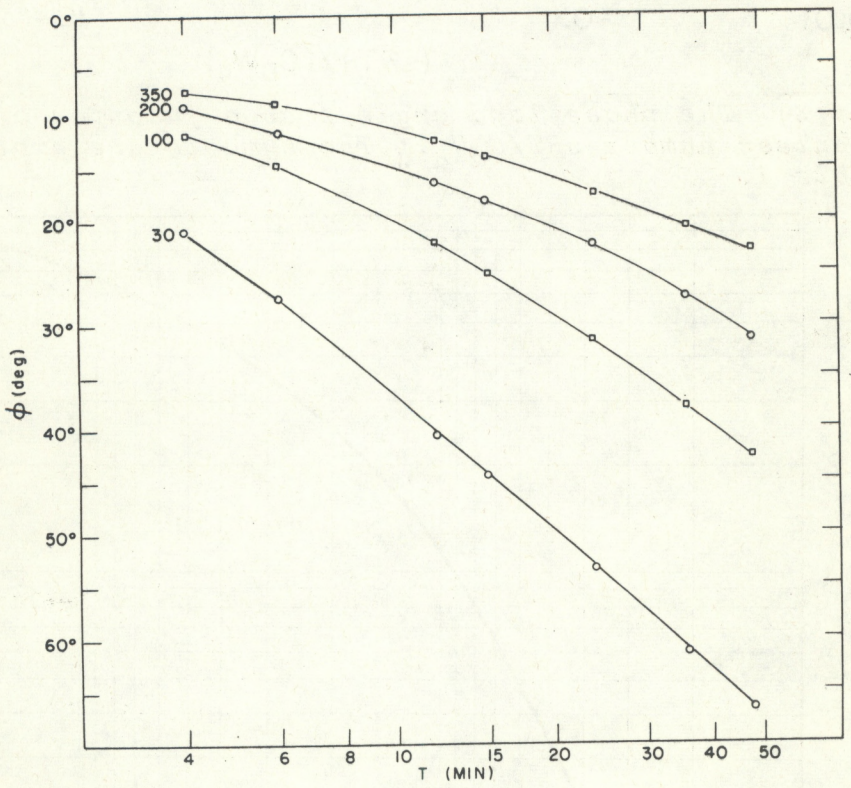

Figure 5: A plot of balloon phase-lead angle (ø) vs. period (T) for the four specific air parcel velocity-amplitude (W_a) classes used in the computations. A drag coefficient of 0.8 was used throughout.

The speed amplitude ratio W_b/W_a as a function of period T for the four values of W_a is shown in figure 6, all curves intersect at T = 9 min., meaning that the velocity ratios are identical at that point regardless of the air-parcel velocity-amplitude, W_a. The relatively-high ratio W_b/W_a of the balloon with W_a = 30 cm sec^{-1} for periods less than about 6 minutes is probably due to resonance with the Brunt-Vaisala period. With the exception of velocity amplitude of 30 cm s^{-1}, the ratio W_b/W_a is nearly independent of velocity amplitude from T = 4 to 12 minutes.

For the cases considered here, balloon velocity-amplitude efficiency is good for a wide range of period and W_a, being greater than 85% for W_a greater than 100 cm sec^{-1} and T less than 36 minutes.

The ratio of the balloon height amplitude to air-parcel amplitude (A_b/A_a) is plotted as a function of period in figure 7. The lines intersect, much as in figure 6, but at about T = 7 minutes. In the region from T=4 to 10 min., the amplitude ratio appears nearly independent of W_a and period(except for W_a=30 cm s^{-1})because of the shallow slopes of the curves. However, $\Delta(A_b/A_a)/\Delta T$ decreases continuously as period increases while $\Delta(A_b/A_a)/\Delta W_a$ increases as period increases. The amplitude ratios are generally a little smaller than velocity-amplitude ratios for any given combination of T and W_a. The curve for W_a = 30 cm sec^{-1} is virtually exponential, as in figure 5. Balloon amplitudes are greater than 80% of air-parcel amplitudes for all periods less than 36 minutes and all W_a greater than 100 cm sec^{-1}.

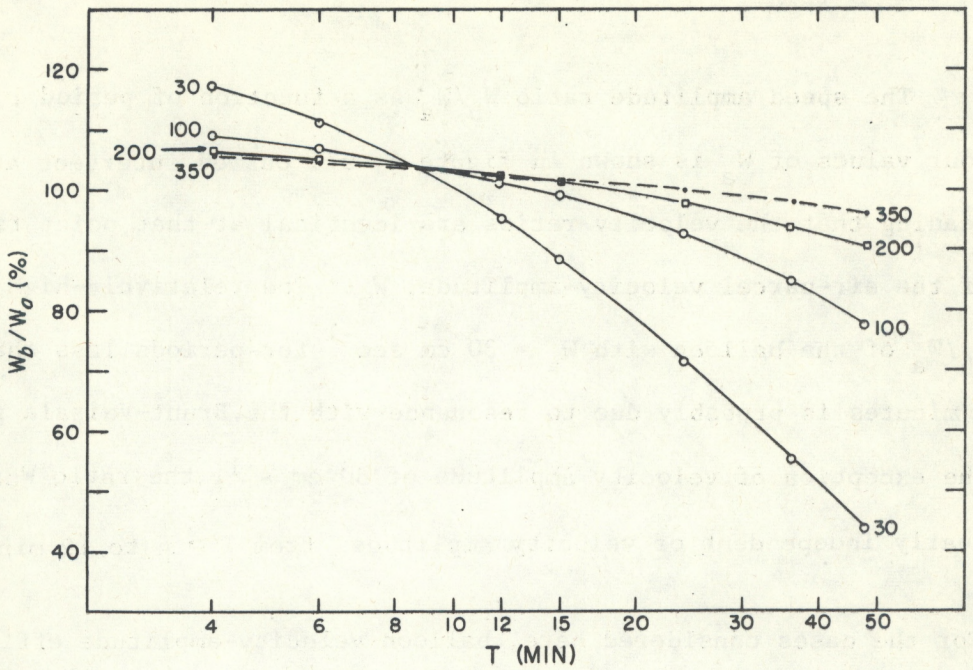

Figure 6: Ratio of balloon to air parcel vertical velocity amplitude (W_b/W_a), expressed as a percent, vs. period (T) for the four velocity-amplitude (W_a) classes used in figure 5. Note the relative insensitivity of the ratio W_b/W_a to velocity amplitude (W_a) for T<12 minutes (except) for W_a= 30 cm s^{-1}).

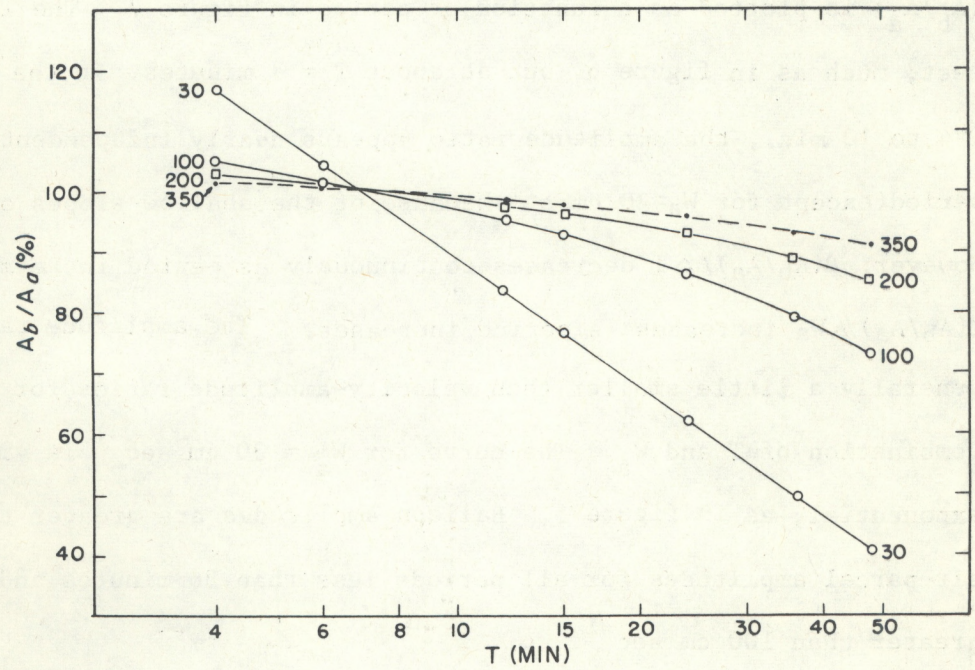

Figure 7: Ratio of balloon to air parcel amplitude (A_b/A_a) (in terms of a percent) vs. period (T) for the four velocity-amplitude classes of figure 5. The results are similar to those of figure 6.

Table 2. Combination of Balloon Efficiency for Three Drag Coefficients.

Cd	ϕ	Ab/Aa	Wb/Wa
T = 12 minutes, Aa = 400 meters, Wa = 3.0 m s^{-1}			
0.45	16.4°	0.951	1.026
0.80	12.4°	0.968	1.023
1.20	10.1°	0.977	1.020
T = 15 minutes, Aa = 285 meters, Wa = 2.0 m s^{-1}			
0.45	23.6°	0.893	1.000
0.80	18.1°	0.936	1.012
1.20	14.8°	0.953	1.016
T = 48 minutes, Aa = 1600 meters, Wa = 3.5 m s^{-1}			
0.45	31.8°	0.812	0.908
0.80	24.2°	0.885	0.960
1.20	20.0°	0.915	0.981
T = 36 minutes, Aa = 345 meters, Wa = 1.0 m s^{-1}			
0.45	48.7°	0.624	0.732
0.80	38.1°	0.748	0.849
1.20	23.7°	0.814	0.904

A drag coefficient of 0.80 was used on the basis of laboratory measurements by Whannel (1965) and theoretical studies by Hoerner (1958). Yet constant-density balloons are in use whose drag coefficients are larger and smaller than 0.80, depending upon their shape. For example, ellipsoidal balloons, floated with their long axis pointing vertically, have smaller drag coefficients along that axis (the amount depending upon their fineness ratio), and cylindrical balloons, floated with their axis in the horizontal plane, have a drag coefficient of 1.20 perpendicular to the axis. To examine the effect of different drag coefficients, four representative combinations of air velocity-amplitude and period were selected to demonstrate the performances of balloons having drag coefficients of 0.45, 0.80, and 1.20. The results in terms of the three earlier-described efficiency criteria are shown in table 2.

As in figures 3 and 4, the overall effect of increasing the drag coefficient is to decrease the phase-lead angle, increase the percentage of air-parcel amplitude attained by the balloon, and increase, generally, the ratio W_b/W_a. The percentage improvements in efficiency for increasing drag coefficient are greater for the longer periods combined with the smaller W_a values although the absolute efficiency values themselves are smaller. For the shortest period and largest W_a shown in table 2, the ratio W_b/W_a actually decreases slightly with increasing drag coefficient. However, this decrease is towards 1.0, the desired ratio. This occurs at periods close to the natural Brunt-Vaisala period. The results of the drag computations point out the desirability of using a balloon with the highest drag coefficient possible where long-period waves of small amplitude are to be tracked.

All of the performance computations to this point have been made using the parameters of the 60-inch tetrahedral Mylar balloon. As seen in figures 3 and 4, smaller balloons offer the possibility of increased air-motion tracking efficiency by virtue of the increased ratio, frontal-area to mass, contained in the drag term of (3). Since a smaller tetrahedral balloon, 42" on a side, was used earlied by Angell and Pack (1960) for trajectory estimates, characteristic data were available for the smaller balloon. The smaller balloon's norminal volume is 0.32 m^3 (0.322 the volume of the 60" tetroon), its $\Delta Vol/\Delta$ pressure is 1/4.25 that of the 60" tetroon, and the area/volume ratio advantage is 1.37 that of the larger tetroon. The appropriate factors were inserted into (3) and the response of the 42" tetroon was computed for three combinations of period and velocity amplitude. Results are shown in table 3 in comparison with results for the 60" tetroon computed above. The improvement in balloon response is not impressive but the greatest percentage improvement is in the phase-lead angle, amounting to 10 to 12%. A yet smaller balloon would give a greater increase in efficiency. However, the necessity for a 100 gm. payload for tracking purposes (radar transponder) limits the decrease in size for practical use.

It is clear from these specific results that the tetroon used by the Air Resources Laboratories of NOAA do not respond perfectly to vertical air motions typically observed at flight level. However, only for rarely-encountered extreme cases of long periods combined with low vertical speed

Table 3. Comparison of response efficiencies between the 60-inch and the 42-inch tetroons for three different combinations of velocity amplitude and period. A drag coefficient of 0.80 was used.

Balloon (inches)	ϕ	Wb/Wa	Ab/Aa
T = 12 minutes, Wa = 3.5 m s^{-1}			
60	12.4°	1.023	0.981
42	10.9°	1.021	0.984
Percent Increase	12.1	0.0	0.3
T = 24 minutes, Wa = 2.0 m s^{-1}			
60	22.7°	0.978	0.926
42	20.1°	0.986	0.940
Percent Increase	11.5	0.8	1.5
T = 36 minutes, Wa = 1.0 m s^{-1}			
60	38.1°	0.894	0.788
42	34.0°	0.882	0.828
Percent Increase	10.3	3.9	5.1

amplitudes, are the response ratios very low(lead angle over 70°, magnitude ratio W_b/W_a less than 0.4). When response ratios are fairly good, i.e., lead angles are about 20° and A_b/A_a ratios are about 0.80, spectra and co-spectra calculated from these data still differ somewhat from the spectra of the air motions.

4. DEDUCING VERTICAL AIR MOTION FROM BALLOON TRAJECTORIES

It is possible to estimate the true, vertical sinusoidal air motion in which the balloon is floating by observing the balloon's trajectory for one or two cycles and applying appropriate adjustments. This would be particularly useful where the tracking radar is equipped with a real-time analog read-out system. This assumes, of course, a nearly steady-state wave motion in which the balloon is floating. For post-operational analysis it would be more appropriate and accurate to use the tetroon position data as input into (3) and solve for air parcel positions. on the computer. Equation (3) can be re-arranged to solve for air motion acceleration in terms of time-dependent vertical balloon motion. The result is shown below:

$$\ddot{Z}_a = \frac{\ddot{Z}_b(M_b + M_{ap})}{(\rho_a V_b + M_{ap})} - \frac{\rho_a A C_d(\dot{Z}_a - \dot{Z}_b)\left|\dot{Z}_a - \dot{Z}_b\right|}{2(\rho_a V_b + M_{ap})} + \frac{g(M_b - \rho_a V_b)}{(\rho_a V_b + M_{ap})} \qquad (4)$$

It is necessary to select an equilibrium level from the analog flight trace since the equilibrium level for which the balloon was intended does not, for various reasons, always coincide with the average flight level. Since the data available are usually one-minute positions, 30 intermediate points are smoothly-interpolated between the one-minute radar positions by the Curvfit (Akima, 1969) program before processing

by the program representing (4). By beginning the computation at the selected equilibrium level and by assuming no initial relative motion between balloon and the surrounding air, one can estimate the subequent path of the air parcel initially surrounding the balloon for the period that the balloon was tracked. The assumption is also made that the vertical variation of vertical velocity and horizontal wind is zero ($\partial w/\partial z = 0$, $\partial v_h/\partial z = 0$).

Figures 8 and 9 are two examples of air-parcel tracks derived from actual balloon flights in daytime over Columbus, Ohio. The balloon trajectory is shown by the dashed curve and the computed air-motion trajectory by the solid curve. It is noted that the peaks of the long wave air motions lag the peaks of the balloon trajectories in time while the peaks of the short wave air motions show very little lag. This follows from the efficiencies presented in figures 3-7. Figures 8 and 9 show, also, the increasing divergence between balloon and parcel as the wave period increases and as the balloon dwells for extended periods away from its equilibrium level in non-cyclic motion. This is particularly evident in figure 9, between 4 and 10 minutes elapsed time, where the tetroon is suspended at about the same elevation for 6 minutes.

These procedures should be valuable in estimating the spatial relationship between air-motion waves and terrain features over which the low-level air current is flowing and for estimating the true air movement in horizontal boundary-layer helices. It should also be valuable in estimating vertical air speeds at the balloon's position. Furthermore, improved air motion cospectra and spectra should result from the use of air parcel movement derived from (4).

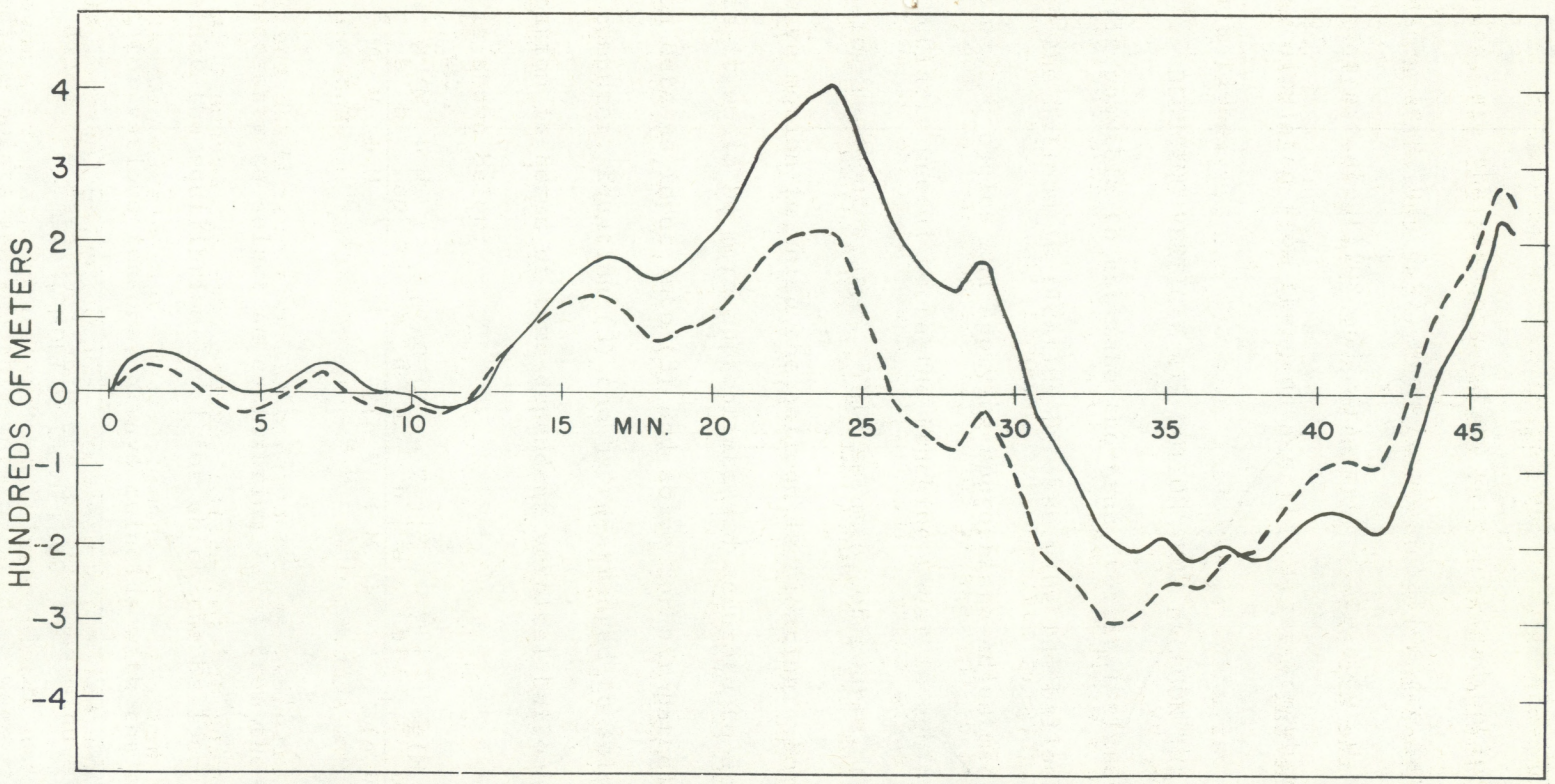

Figure 8: Air parcel trajectory (solid line) derived from radar-tracked tetroon trajectory (dashed line) by the application of (4). The tetroon was floating over Columbus, Ohio, in daytime convective conditions at an average of 300 meters above the terrain. A drag coefficient of 0.8 was used.

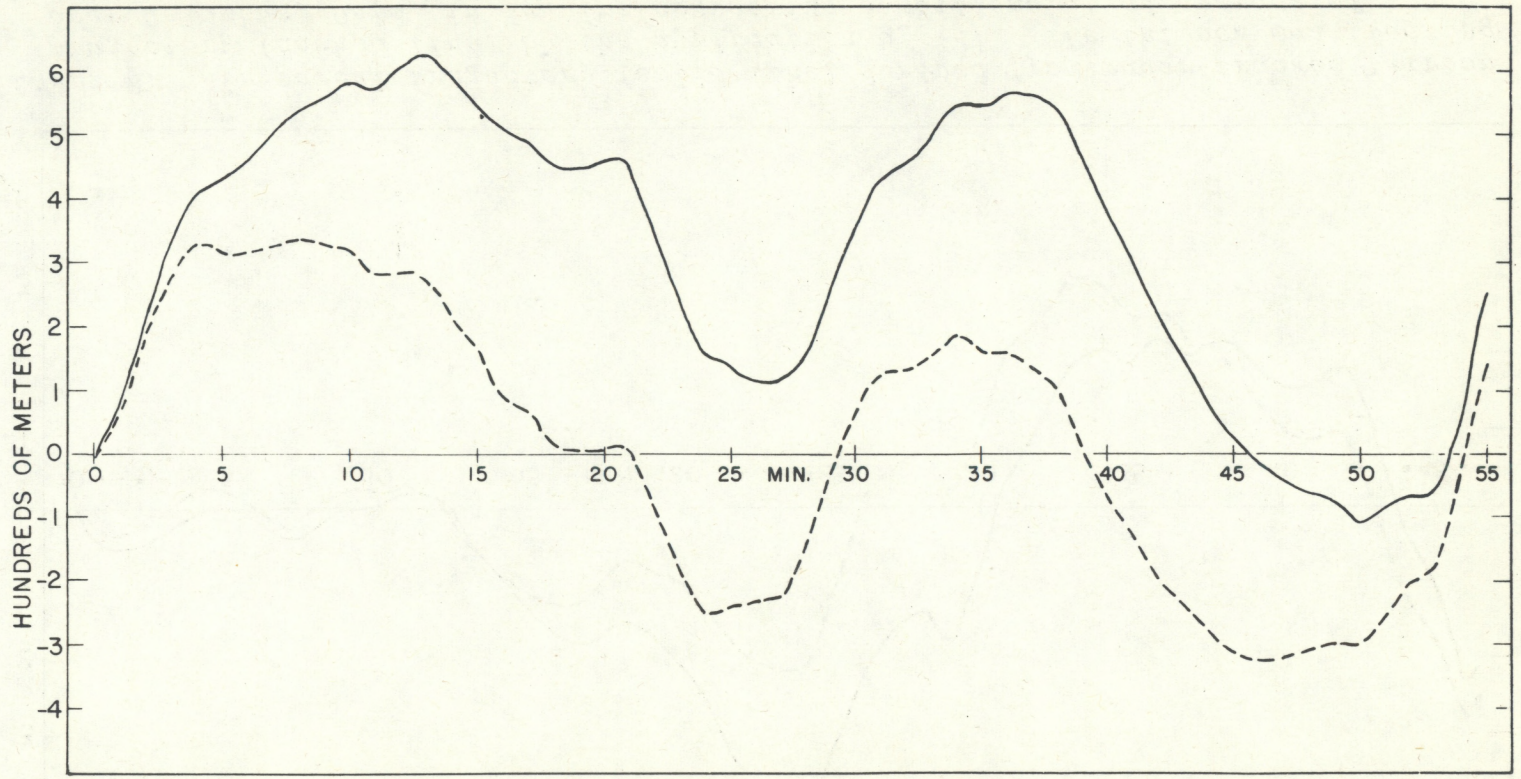

Figure 9: Derived air parcel trajectory from another Columbus, Ohio, flight where the tetroon averaged 400 meters above the terrain. Otherwise, same as figure 8.

5. RESPONSE TO HELICAL AIR MOTIONS

Helices in the planetary boundary layer were observed with neutral (expandable) balloons by Gifford (1953) as early as 1949 and delineated by Pack (1962) with tetrahedral constant-density balloons in 1962. Such helices have been traced by radar-tracked constant-density balloons at various times since then and most recently by Angell et al., (1968) over desert terrain in daytime summer conditions. Because of the importance of such horizontal helices in energy transfers and other boundary layer processes, the theoretical response of these balloons to different types of helices of several sizes and periods of rotation was computed.

In the first type of helix that was considered the current of air was, as before, assumed to move as a whole both laterally and vertically. Consequently, horizontal and vertical balloon motions are a function only of time and not of position. In effect, the simultaneous response of the balloon to vertical and lateral sinusoidal air motions, 90° out of phase, is computed. Representative balloon response to one example of this type of atmospheric helix is shown in figure 10. Because there is no lateral restoring force, the lateral excursions of the balloon closely match those of the air motion regardless of period or amplitude. Note that the balloon assumes an equilibrium trajectory before the end of the first cycle. The ellipticity of the trajectory increases, according to figures 3 and 4, as stability, air period and balloon radius increase, and as drag coefficient and vertical air speed magnitude decrease.

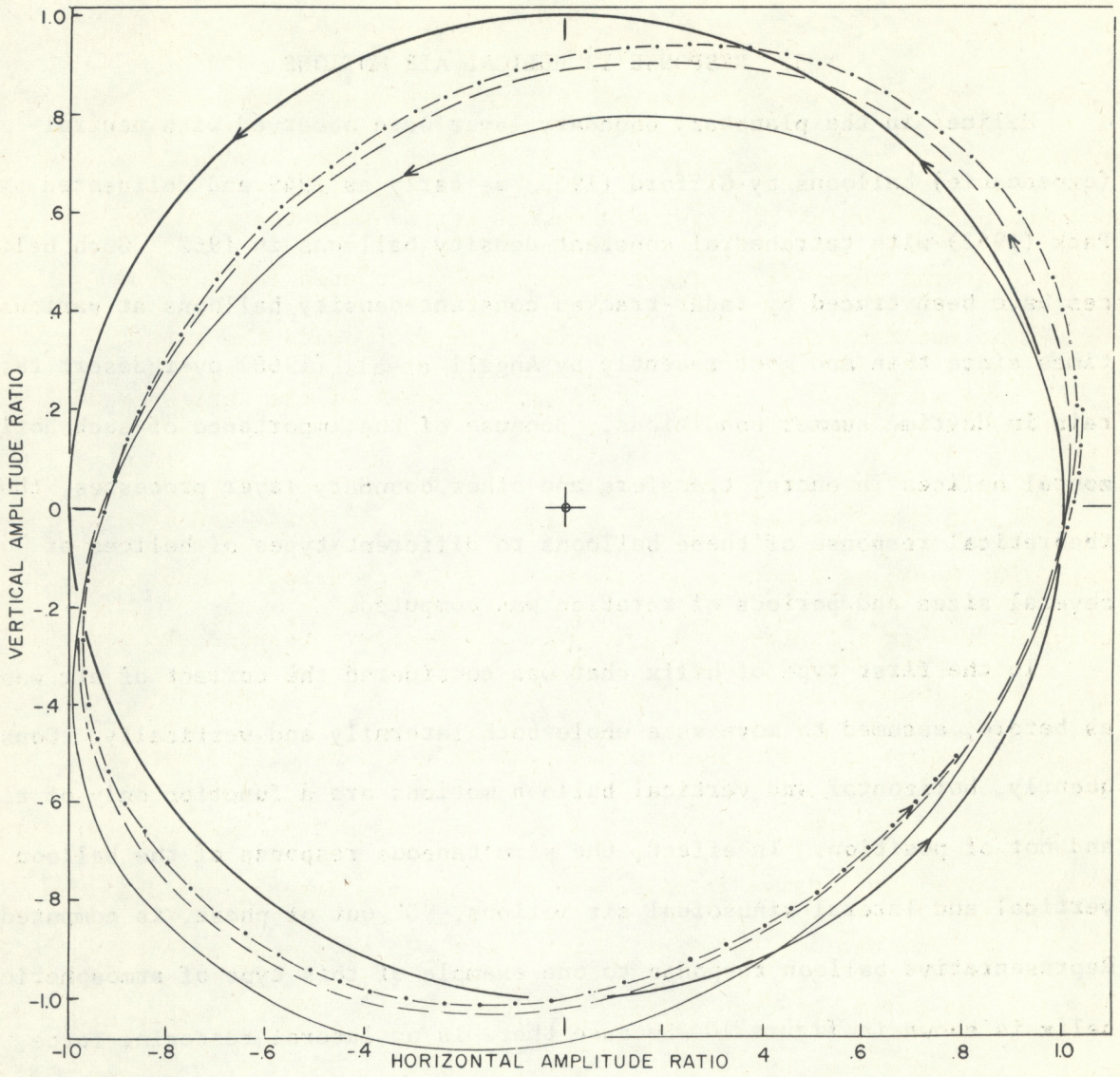

Figure 10: Normalized response of the balloon to the first type of helical air motion described in the text, having an amplitude of 400 m, period of 12 minutes, velocity amplitude of 3.5 m, and balloon drag coefficient of 0.8. The heavy solid line represents the parcel trajectory and arrows show the sense of rotation. The three tetroon (or balloon) cycles are represented respectively by a thin solid line, dashed line, and dot-dash line. Note the slightly elliptical and tilted equilibrium trajectory of the tetroon.

Other types of helices include those characterized by solid rotation or a combination of an outer region of constant circulation and an inner region of solid rotation. Angell et al. (1968; their fig. 6) show evidence that combined helices exist in daytime summer conditions in the southern Idaho desert. In the numerical trajectory that we calculated for a solid rotation helix, the tetroon rather quickly spiraled inward toward the axis. The level of the axis of the helix and the equilibrium level of the tetroon were the same.

For the remainder of the experiments a combined helix was used having a tangential speed of 2 meters per second at 915 meters radius and having a maximum speed at a radius of 270 meters. This size and speed are compatible with the average helix observed by Angell et al. (1968; their fig. 5). The initial position of the tetroon was always at a radius of 915 meters.

In the first experiment with the combined helix, the balloon's starting position, its equilibrium level, and the helix axis were all at the same elevation. The balloon spiraled toward the helix axis, but much more slowly than for the solid rotation helix. Its path is shown in figure 11 along with a graph of the radial variation of the tangential speed. In 2880 sec the hypothetical balloon was only a few meters from the helix axis. Since the helix axis and the tetroon's equilibrium level would hardly ever be at the same elevation, a trajectory was computed with the balloon's equilibrium level 600 m below both the helix axis and the balloon's starting elevation. The change in balloon trajectory is marked as shown in figure 12. In the same elapsed time, 2880 sec, the balloon is now 240 m from the helix axis and the spirals of the trajectory are bunched around the radius of maximum tangen-

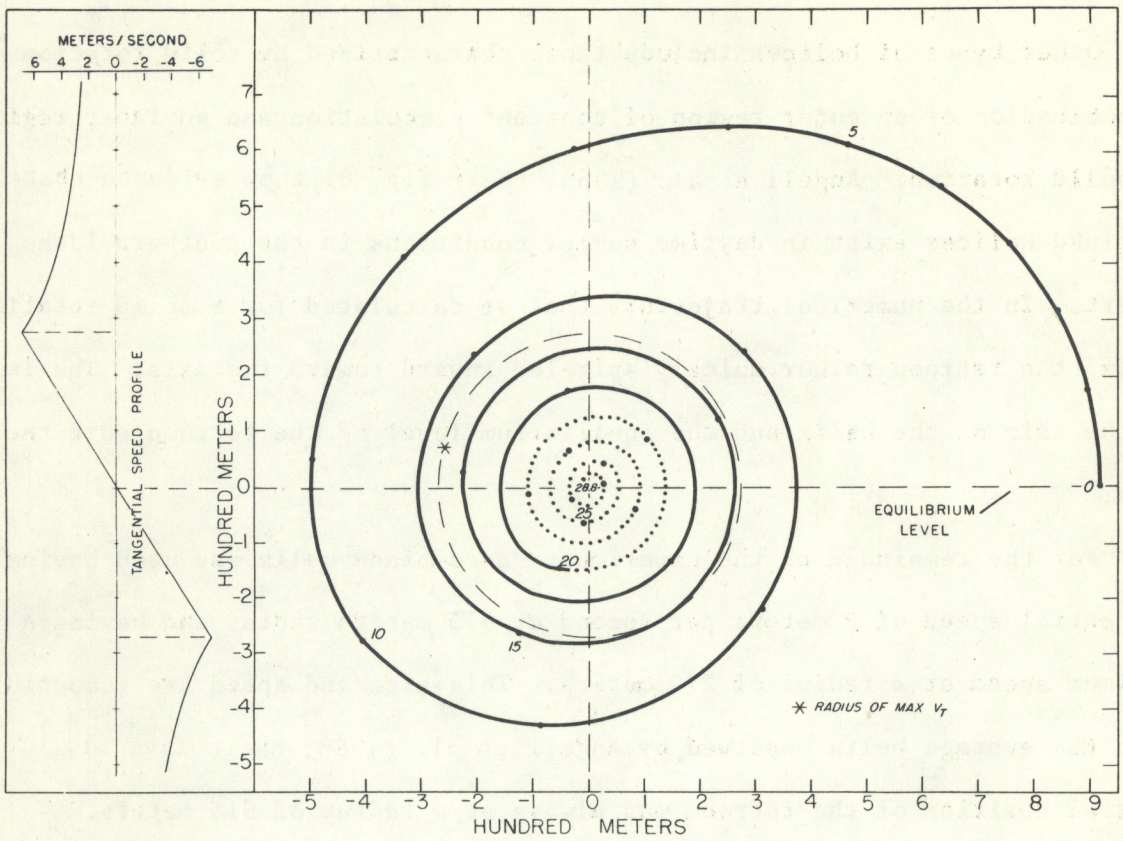

Figure 11: Reaction of tetroon in a horizontal combination helix. The tangential speed (V_t) distribution is shown in the left side of the figure. The elapsed time for each 500 sec (8-1/3 min) is noted. Additional details are in the text.

tial speed (located by the dashed circle). This experiment shows the strong control exerted on the tetroon trajectory by a displaced balloon-equilibrium-level. Also it strongly suggests that the tetroon's equilibrium level is generally somewhat below the axis of helices delineated by tetroons in field experiments since tetroons are seldom tracked into tight spirals as in figure 11. In actual field programs the tetroon is launched from the ground and so enters a helix, if encountered, from below. The last computation simulates this condition by starting the tetroon 915 m directly below the helix axis

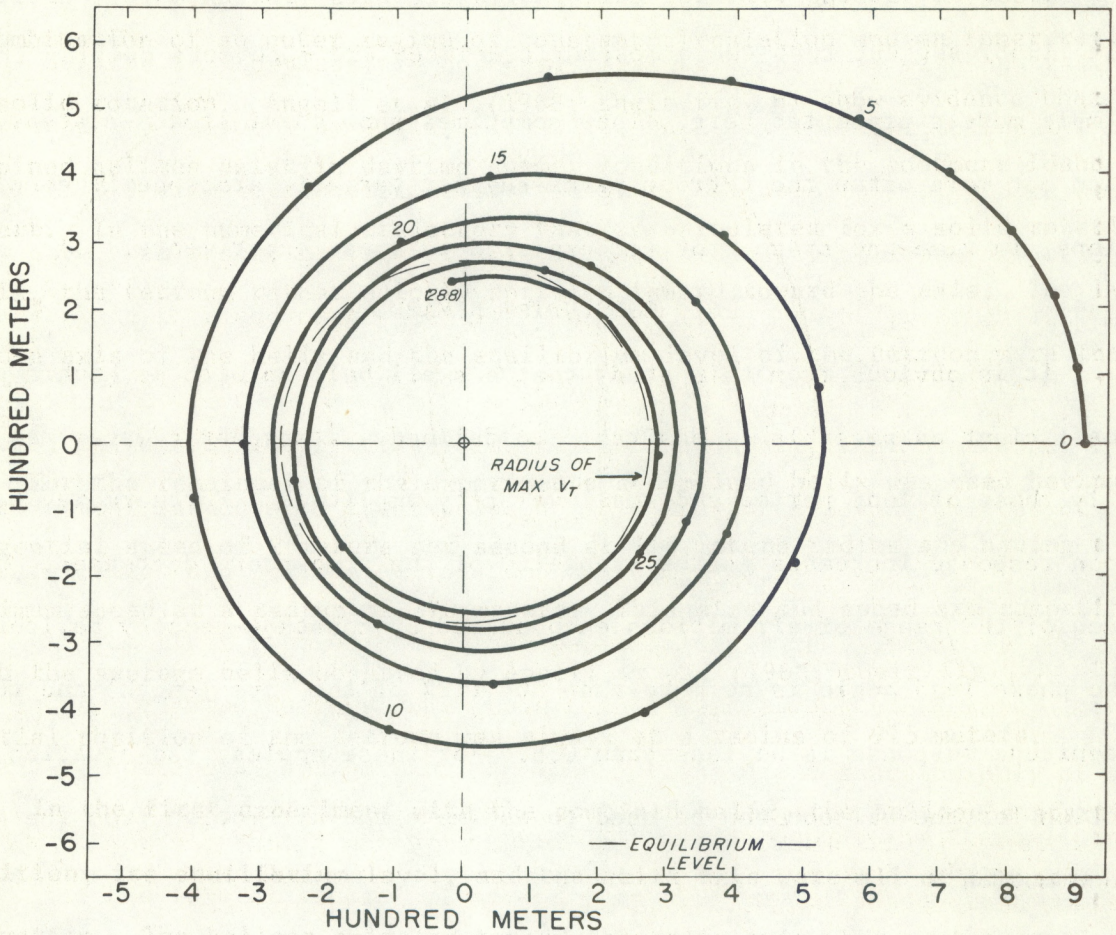

Figure 12: Same as figure 11 but the tetroon equilibrium level causes a marked changed in the tetroon's spiral pattern.

with the tetroon's equilibrium level again 600 m below the axis. The result displayed in figure 13 is an increase in the average radius of the inward spiral over that in figure 12, and so in 2880 sec the balloon makes fewer turns around the axis and arrives at a larger radius (275 m) in the given time.

Observed lateral-vertical tetroon trajectories (for example, Angell et al., 1968) suggest that the atmospheric helices are much more complex than the simple models presented here. They sometimes show quasi-steady-state rotation but more often the tetroon paths suggest variable atmospheric conditions, in time and space, not yet explored in these experiments.

6. CONCLUDING REMARKS

It is obvious from this study that a small balloon with as high a drag coefficient as possible is desirable to delineate atmospheric waves, especially those of long period and small velocity amplitude. Furthermore, balloon response increases as the stability of the atmosphere decreases. Over much of the range of air motions encountered by constant-density balloons, the phase lead angle is no more than 30° (12% of the wave length) and the magnitude response is no less than 0.8. For these scales, the equation of motion for the balloon can be used to estimate the air motion from the balloon motion.

The response of balloons to helical air motions depends greatly on the characteristics of the helix (e.g., solid rotation, constant circulation, etc.). In some cases, the balloon spirals to the center of the helix. Further research should be concerned with the dynamics of these helices and with estimating their size and speed of rotation from observed constant-density balloon trajectories.

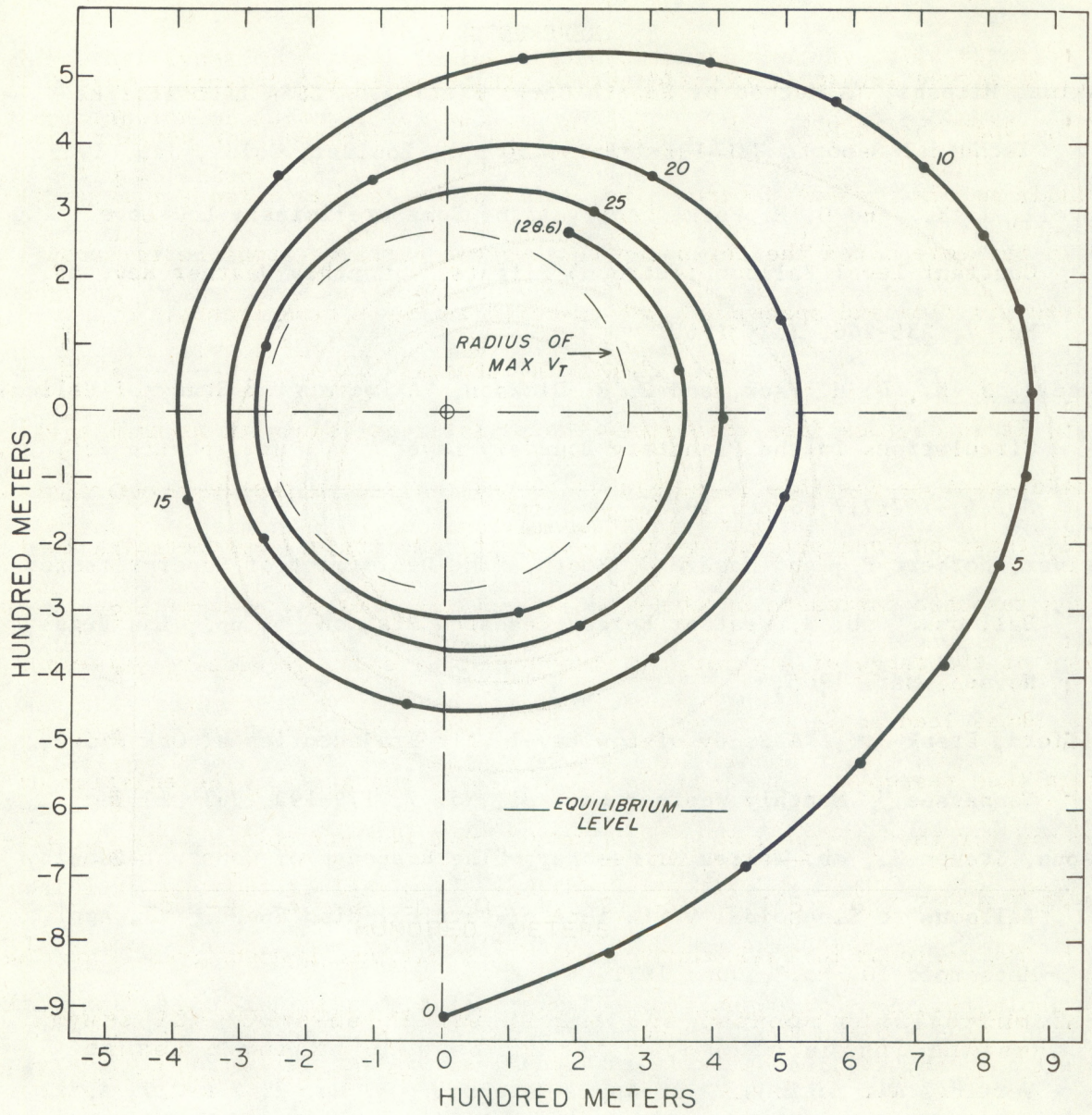

Figure 13: Same as figure 12 except that the tetroon is started 915 meters directly below the helix axis. The tetroon makes fewer turns around the axis in the given time of 2880 sec.

7. ACKNOWLEDGEMENTS

The authors wish to acknowledge the many helpful suggestions given by Dr. James K. Angell and Mr. Donald H. Pack during the preparation of this material. Mr. Anthony Giarrusso made the project possible by his computer programming assistance.

8. REFERENCES

Akima, Hiroshi, "A Method of Smooth Curve Fitting." ESSA Laboratories Technical Report, ERL 101-ITS 73, 30 pp., Boulder, Colo., Jan. 1969.

Angell, J. K., and D. H. Pack, "Analysis of Some Preliminary Low-Level Constant Level Balloon (Tetroon) Flights." Monthly Weather Rev. 88, No. 7, 235-246, July 1960.

Angell, J. K., D. H. Pack, and C. R. Dickson, "A Lagrangian Study of Helical Circulations in the Planetary Boundary Layer." J. Atmospheric Sci. 25, No. 5, 707-717, Sept. 1968.

Delver, Norbert F., and Howard G. Booth, "The Deployment of Superpressured Balloons." U. S. Weather Bureau Research Station, 59 pp., Las Vegas, Nevada, Mar. 1965.

Gifford, Frank Jr., "A Study of Low Level Air Trajectories at Oak Ridge, Tennessee." Monthly Weather Rev. 81, No. 7, 179-192, July 1953.

Hanna, Steven R., and Walter H. Hoecker, "The Response of Constant-Density Balloons to Sinusoidal Variations of Vertical Wind Speed." J. Appl. Meteorol. 10, No.3, June 1971.

Hirsch, John H., and Ray D. Booker, "Response of Superpressure Balloons to Vertical Air Motions." J. Appl. Meteorol., 5, No. 2, 226-229, April 1966.

Hoerner, S. F., "Fluid-Dynamic Drag." Published by the author at Midland Park, New Jersey, 1958.

MacCready, Paul B. Jr., and Henry R. Jex, "Study of Sphere Motion and Balloon Wind Sensors." Meteorology Research Inc., for Aero-Astrodynamics Laboratory, Geo. C. Marshall Space Flight Center, NASA Tech. Memo. X-53089, 39 pp., July 1964.

Mangold, Edward C., "Investigation of the Use of Balloons for Atmospheric Turbulence Measurement." Research Foundation, Okla. State University, Weather Bureau Grant-56, for ESSA, Dept. of Commerce, 79 pp., April 1966.

Pack, Donald H., "Air Trajectories and Turbulence Statistics from Weather Radar Using Tetroons and Radar Transponders." Monthly Weather Rev., 90, No. 12, 491-506, Dec. 1962.

Prandtl, Ludwig, "Essentials of Fluid Dynamics." Hafner Publishing Co., New York, N. Y., 452 pp., 1952.

Reed, Wilmer H. III, "Dynamic Response of Rising and Falling Balloon Wind Sensors with Application to Estimates of Wind Loads on Launch Vehicles." NASA Tech. Note - D-1821, 31 pp., Langley Research Center, Langley Station, Hampton, Va., October 1963.

Scoggins, James R., "Sphere Behavior and the Measurement of Wind Profiles." NASA TN-D-3994, 53 pp., Geo. C. Marshall Space Flight Center, Huntsville, Alabama, June 1967.

Vergeiner, I., and D. K. Lilly, "The Dynamic Structure of Lee Wave Flow As Obtained from Balloon and Airplane Observations." Monthly Weather Rev., 98, No. 3, 220-232, Mar. 1970.

Whannel, Paul R., "Aerodynamic Characteristics of Tetrahedrons." GCA Viron Div., GCA Corp., Minneapolis, Minn., prepared for Weather Bureau under contract Cwb-11054, 16 pp., Washington, D. C., Nov. 1965.